Boundary-Layer Meteorol (2008) 126:365–388
DOI 10.1007/s10546-007-9238-x

ORIGINAL PAPER

Flow in a Street Canyon for any External Wind Direction

Lionel Soulhac · Richard J. Perkins · Pietro Salizzoni

Received: 7 March 2007 / Accepted: 15 October 2007 / Published online: 7 November 2007

Abstract An analytical model has been developed for the flow along a street canyon (of height H and width W), generated by an external wind blowing at any angle relative to the axis of the street. Initially, we consider the special case of a wind blowing parallel to the street. The interior of the street is decomposed into three regions, and the flow within each region is assumed to depend only on the external wind and the distance to the closest solid boundary. This decomposition leads to two different flow regimes: one for narrow streets ($H/W > 1/2$) and one for wide streets ($H/W < 1/2$). The theoretical model agrees well with results obtained from numerical simulations using a Reynolds-Averaged Navier–Stokes model. We then generalize the model to the case of arbitrary wind direction. Numerical solutions show that the streamlines of the mean flow in the street have a spiral form, and for most angles of incidence, the mass flux along the street scales on the component of the external wind resolved parallel to the street. We use this result to generalize the model derived for wind blowing parallel to the street, and the results from this model agree well with the numerical simulations. The model that has been developed can be evaluated rapidly using only very modest computing power, so it is suitable for use as an operational tool.

Keywords Numerical modelling · Street canyon · Urban canopy flow

1 Introduction

There are many practical situations where it would be useful to be able to compute pollutant concentrations in a network of streets within an urban area. Local authorities need

L. Soulhac (✉) · R. J. Perkins · P. Salizzoni
Laboratoire de Mécanique des Fluides et d'Acoustique, UMR CNRS 5509, University of Lyon – Ecole Centrale de Lyon, INSA Lyon, Université Claude Bernard Lyon I, 36, Avenue Guy de Collongue, 69134 Ecully, France
e-mail: lionel.soulhac@ec-lyon.fr

P. Salizzoni
DIASP Politecnico di Torino, Corso Einaudi, 24 Torino, Italy

such information, for example, for a better understanding of the impact of urban air quality on health, and for the assessment of the likely impact of urban planning and traffic control measures on population exposure and health.

As a general rule, urban air quality depends on the transport and dispersion of pollutants in the atmospheric boundary layer, and involves motions on a wide range of length and time scales, ranging from the scale of the continent to the scale of the street. But within individual streets, the close proximity of emitters (vehicle exhausts, for example) and receptors means that a significant proportion of the pollution comes from within the street, and depends on very local characteristics. The flow within the street, which is generated by the wind blowing at roof level, therefore plays an important role in determining pollutant concentrations within the street, and it is reasonable to suppose that a model for pollutant concentrations in city streets could be constructed by considering how the pollutants emitted from local sources are transported and dispersed by the flow generated within the streets by an external wind blowing at roof level.

For several years we have been developing an operational model—SIRANE—based on this idea. Pollutant concentrations in a network of city streets are computed as a function of the street geometry, the external meteorological conditions and the local emissions. Some results of that model, applied to specific sites, can be found in Soulhac et al. (2003). There are two essential components of this model: the first concerns the transport and dispersion of pollutants within a city street, for any wind direction relative to the street axis, and the second concerns the way in which mass transfer occurs at street intersections. The calculation of the mass transfer at a street intersection requires a reliable estimate of the fluxes entering and leaving the intersection from the different intersecting streets, so a major requirement for the street model is that it should provide a good estimate of the mass flux along the street.

There have been numerous studies over the last 30 years aimed at studying the transport and dispersion of pollutants in individual streets. In most of these studies it has been assumed that the street is long compared with its width, so that the flow can be considered two-dimensional. Most of the studies have been devoted to the particular case of a wind blowing perpendicular to the street, probably because it is widely believed that this configuration maximises the retention time of the pollutants in the street. In fact, several field experiments have demonstrated that this is not necessarily correct. If the street is sufficiently long, the wind blowing along the street causes an accumulation of pollutants, and the resulting concentration at the downwind end of the street can exceed that produced when a similar wind blows across the street (Baranger 1986; Berkowicz et al. 1994, 1996).

When the wind blows perpendicular to the street, the flow within the street depends on the external wind speed and the street geometry; for a street bounded by buildings of approximately equal height, the street geometry can be characterized by its width W and its height H. Based on the wind-tunnel measurements of Hussain and Lee (1980), Oke (1988) proposed that the flow could be classified into three regimes, depending on the aspect ratio H/W. For very wide streets ($H/W < 0.15$) the buildings act as isolated roughness elements, and the flow within the street is similar to that in the wake of an isolated obstacle: this regime is referred to as the isolated roughness regime. At intermediate aspect ratios ($0.15 < H/W < 0.65$) the street width is comparable to the size of the recirculating region behind the obstacle, and there is therefore interaction between the two sides of the street: this regime is known as the wake interference regime. For very narrow streets ($H/W > 0.65$) the external flow does not penetrate into the street, but generates a recirculating cell: this is known as the skimming flow regime (Albrecht 1933). If the buildings that define the street are not symmetrical, or if the street is narrow ($H/W \geq 3/2$), then two counter-rotating cells may form instead of one (Hoydysh and Dabberdt 1988; Rafailidis 1997; Hassan and Crowther 1998; Soulhac 2000).

The recirculating flow within the street determines how pollutants are mixed within the street, and in particular the rate at which pollutants are transferred from street to roof level and vice versa. The presence of two counter-rotating cells reduces this transfer rate dramatically, e.g. (Soulhac 2000). The exchange between the air within the street and the overlying atmosphere depends on the turbulent flux across the shear interface between the two regions, so the average concentration within the cavity depends on the interaction between the recirculating flow and the entrainment across the interface; see, for example, Salizzoni (2006).

There are only a few studies of the flow induced in a street by an external wind blowing at an arbitrary angle, and the results are somewhat contradictory. If the angle between the wind direction and the street axis is defined as θ_∞ (so that $\theta_\infty = 0$ corresponds to a wind parallel to the street), then for $\theta_\infty > 20°$ the streamlines within the street form a helicoidal pattern (Yamartino and Wiegand 1986). Field experiments conducted by Takahashi et al. (1996) show that the angular velocity of the spiral increases in proportion to $\sin(\theta_\infty)$. Observations suggest that the spiral is not regular, and that the orientation of the streamlines at ground level θ_{ground} differs from the orientation at roof height θ_H. On the basis of field measurements, Nakamura and Oke (1988) concluded that $|\,\theta_{\text{ground}}\,| < |\,\theta_H\,|$ whereas the wind-tunnel measurements of Dabberdt and Hoydysh (1991) suggest that $|\,\theta_{\text{ground}}\,| > |\,\theta_H\,|$. Field measurements made by Rotach (1995) showed that the turbulent intensities within a real street are fairly insensitive to the direction of the external wind. More recently, in the DAPPLE project, Dobre et al. (2005) measured the flow within a street in London, for arbitrary external wind direction, and based on these measurements, they concluded that the flow in the street can be described as a superposition of a transverse flow driven by the perpendicular wind component, and a longitudinal flow driven by the along-street component.

Various models for flow and dispersion in urban streets have been proposed, based essentially on two different approaches, and with two different objectives. There have been several simulations of flow in street cavities, using numerical models based either on the Reynolds-Averaged Navier–Stokes equations (Johnson and Hunter 1995; Hassan and Crowther 1998) or on large-eddy simulation, e.g. Ca et al. (1995); Walton et al. (2002). In this approach the whole of the street is discretised, and the velocity and concentration fields are calculated at every node of the grid. Such calculations require large amounts of computing resources, and are not feasible for operational calculations, which have to be performed for a wide range of conditions and street geometries, using more modest computing power. So simpler operational models have been developed, which seek to compute a more limited number of relevant variables, more rapidly. Typical examples include APRAC/STREET (Johnson et al. 1973), CPBM (Yamartino and Wiegand 1986), CAR (Eerens et al. 1993) and OSPM (Hertel and Berkowicz 1989). These models are essentially based on a combination of analytical and empirical formulations for the flow field within the street, for the two asymptotic conditions of wind perpendicular to the street and wind parallel to the street. For the wind blowing parallel to the street it is generally assumed that the wind profile has a logarithmic form, although this has still to be verified. The general case of an arbitrary wind direction is then computed by considering linear superposition of the two asymptotic solutions. It has yet to be shown that this superposition is justified, and that there is no non-linear interaction between the two components of the velocity field.

In Sect. 2, we present a new model for flow in a street generated by a wind blowing parallel to the street axis. The results are compared with the results from a numerical simulation of the flow, computed using a Reynolds-Averaged Navier–Stokes model. In Sect. 3 the numerical simulations are used to investigate the influence of wind direction on the flow in the street. The flow pattern generated by the wind has a spiral form, and the non-linear interaction of the cross-street component with the component along the street modifies the profile of the

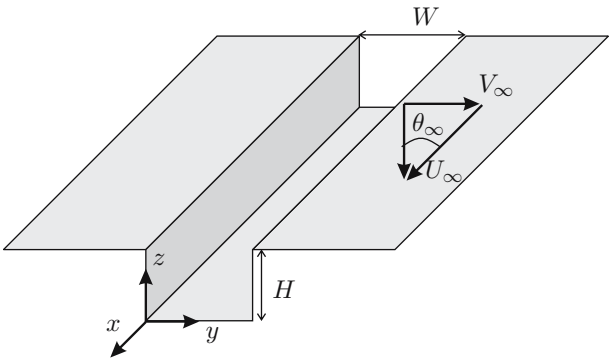

Fig. 1 Street geometry and co-ordinate system

longitudinal velocity considerably. Nevertheless the spatially-averaged longitudinal velocity is relatively unchanged, and scales on the component of the external wind resolved parallel to the street. This allows us to generalize the model derived in Sect. 2 for the case of a wind blowing at an arbitrary orientation to the street axis. The results from this generalized model again agree well with the results from numerical simulations.

2 External Wind Parallel to the Street Axis

2.1 Theoretical Model

We consider here an infinitely long two-dimensional symmetrical street, characterized by its height H and width W (see Fig. 1). The coordinate system is defined in Fig. 1; the origin is located at the street level, at one side of the street, and the x-axis is oriented parallel to the street. Then the inside of the street corresponds to the origin $0 \leq y \leq W,\ 0 \leq z \leq H$.

The mean velocity components in the directions x, y and z are denoted by $\overline{u}$, $\overline{v}$ and $\overline{w}$, respectively. The aerodynamic roughness of the side walls and floor of the canyon will be characterized by a roughness length z_i. The main assumption of the model is that the mean velocity field within the street (for $z < H$) is induced by a momentum transfer from the external flow; the incoming momentum is due only to turbulent entrainment, and this can be expressed by the shear stress τ_H, exerted by the external flow at roof level.

It is assumed that the street under consideration is placed within an urban canopy made up of a group of buildings. The surface layer (SL) developing above the urban canopy is made up of two different regions: the roughness sub-layer (RSL) and the inertial region (IR). The flow within the RSL is influenced by the wakes of individual buildings, so it will not be homogeneous in the horizontal plane (Raupach et al. 1980; Rotach 1993). On the other hand, the flow within the IR is homogeneous in the horizontal plane and the mean velocity profile can be described by means of the classical logarithmic law:

$$\overline{u} = \frac{u_*}{\kappa} \ln\left(\frac{z-d}{z_0}\right), \tag{1}$$

where u_* is the friction velocity, which is a measure of the shear stress magnitude τ_0 within the inertial region ($\tau_0 = \rho u_*^2$, where ρ is the air density), d is the displacement height, z_0 is the aerodynamic roughness of the surface of the urban canopy and κ is the von Kármán

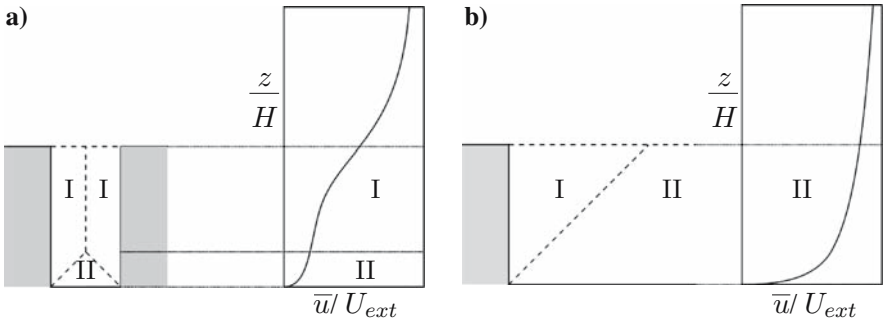

Fig. 2 Flow regimes in a street parallel to the wind direction: influence regions and mean velocity profiles. (**a**) Narrow street: $H/W > 0.5$, (**b**) Wide street: $H/W < 0.5$

constant. The parameters d and z_0 depend on the geometrical characteristics of the surface considered at a scale that is large compared with that of the street (the district or urban scales, for example). These two parameters can then be treated as constant values and estimated as a function of the geometrical characteristics of the size and orientation of the buildings (Bottema 1997; MacDonald et al. 1998; Grimmond and Oke 1999). Once d and z_0 have been evaluated and once the mean wind speed U_{ext} at a given height z_{ext} (within the IR) has been estimated, u_* (and hence τ_0) can be determined using Eq. 1.

The relation between τ_H and τ_0 within the RSL is more difficult to obtain. Results of a field measurement campaign by Rotach (1993) revealed that the Reynolds stress decreased within the RSL with decreasing distance from the ground. Results obtained by Rafailidis (1997) and MacDonald et al. (2000) suggest that the stress decrease mainly takes place below the roof level. Other experimental results obtained by Cheng and Castro (2002) showed that the spatially-averaged stress within the RSL is constant with height right down to the top of a cubical building array. In order to model the mean flow within the canopy, MacDonald (2000) assumed a constant value of the Reynolds stress, which makes it possible to match the velocity profile at the top of the canopy with the mean profile in the IR. We will adopt the same assumption, so that $\tau_H = \tau_0$.

2.1.1 Flow Regimes for an External Wind Aligned with the Street Axis

The flow within the street is driven by the external flow and is determined by the incoming momentum at the roof height, due to turbulent entrainment. The no-slip condition is imposed on the internal faces of the canyon and this generates boundary layers along the walls and the floor. In order to simplify the problem, we shall not consider the interaction between the different boundary layers and we shall assume simply that each surface influences the flow in part of the canyon. This is shown schematically in Fig. 2, for a narrow street (Fig. 2a) and a wide street (Fig. 2b). The region of the flow influenced by the side walls is denoted Region I and the region influenced by the ground, Region II. The boundaries between the regions are defined geometrically, such that any point on a boundary between two regions is equidistant from the two surfaces that generate the two regions. Then it follows that for both regime types the boundary-layer thickness is given by $\delta_i = min(H, W/2)$. It is worth noting that the relative importance of Regions I and II depends on the street geometry, in particular on the street aspect ratio H/W. It follows from this that there are two basic flow regimes:

– *Narrow street regime:* $H/W > 0.5$ and $\delta_i = W/2$
For a narrow street, the vertical walls contribute more than the half of the total street perimeter and most of the flow within the street is therefore controlled by the side walls. The influence of the ground is confined to the lower part of the flow field. The mean velocity profile in the street centre can be considered as composed of two different regions (Fig. 2a), and it will be shown that, in Region I, the mean velocity profile can be modelled by means of an exponential law, whilst in Region II, a logarithmic law needs to be adopted.

– *Wide street regime:* $H/W < 0.5$ and $\delta_i = H$
For a wide street, the length of the lower boundary exceeds the half of the street perimeter; the influence of the lateral walls is weaker and the flow dynamics are dominated by the influence of the lower boundary.

In order to model the flow within the street, the dynamics of each region will be considered as independent from the others.

2.1.2 Region I: Region of Influence of the Side Walls

We first consider the region within which the velocity field is mainly influenced by the side walls, in the narrow street regime ($z > \delta_i$). As already mentioned, the dynamics of this region are assumed to be independent of the rest of the velocity field, i.e., we neglect the influence of the ground on this region. So the configuration that is actually modelled here is that of flow between two parallel vertical planes (separated by a horizontal distance W), and driven by an external wind at roof level, parallel to the planes. The momentum transfer from this external flow takes place through turbulent entrainment across a shear layer at the interface, and this is resisted by the drag on the vertical walls, which are assumed to be aerodynamically rough.

No transverse component of the flow within the street is considered ($\overline{v} = 0$ and $\overline{w} = 0$) and the longitudinal component is assumed to be uniform ($\partial\overline{u}/\partial x = 0$) and stationary ($\partial\overline{u}/\partial t = 0$). Given these conditions, the Navier-Stokes equations can be reduced to the component parallel to the x direction:

$$\frac{\partial \overline{u'v'}}{\partial y} + \frac{\partial \overline{u'w'}}{\partial z} = 0. \tag{2}$$

The Reynolds stress in Eq. 2 is modelled by using a gradient diffusion law with a turbulent diffusivity, K, and the momentum balance then becomes:

$$\frac{\partial}{\partial y}\left(K\frac{\partial \overline{u}}{\partial y}\right) + \frac{\partial}{\partial z}\left(K\frac{\partial \overline{u}}{\partial z}\right) = 0. \tag{3}$$

This equation can be written in dimensionless form:

$$\frac{\partial}{\partial y^+}\left(K^+\frac{\partial u^+}{\partial y^+}\right) + \frac{\partial}{\partial z^+}\left(K^+\frac{\partial u^+}{\partial z^+}\right) = 0, \quad \text{with} \begin{cases} y = \delta_i y^+ \\ z = \delta_i z^+ \\ \overline{u} = U_m u^+ \\ K = K_m K^+ \end{cases} \tag{4}$$

where δ_i represents the thickness of the boundary layer developing on the side walls and U_m and K_m are the velocity magnitude and the turbulent diffusivity on the centreline at the interface, i.e., at $y = \delta_i$ and $z = H$. To solve Eq. 4, we use the method of the separation of variables, and we assume that u^+ and K^+ can be expressed as follows:

$$u^+ = f(y^+)g(z^+), \tag{5}$$

$$K^+ = y^+ g(z^+). \tag{6}$$

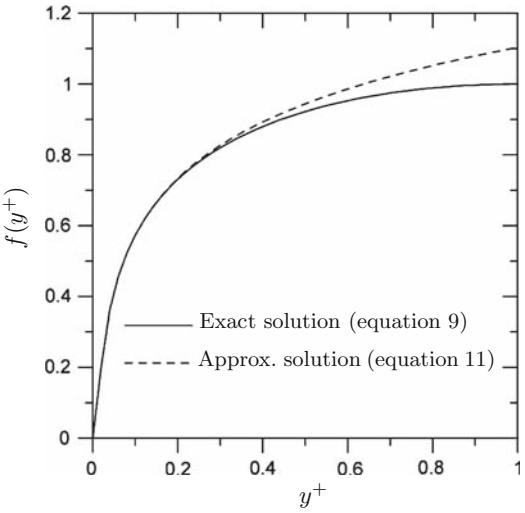

Fig. 3 Form function for the horizontal profile of the mean velocity in Region I

The functions f and g represent the horizontal and vertical variations of u^+. We have assumed that the vertical variation of K^+ is similar to that of u^+, defined by g (hypothesis derived from the similarity of the two profiles). The horizontal variation is considered as proportional to the distance from the wall y^+, as is generally assumed for a turbulent boundary layer. Substituting Eqs. 5 and 6 into (4), we obtain a differential equation in f and g:

$$f'g^2 + y^+ f''g^2 + y^+ fgg'' + y^+ fg'^2 = 0. \tag{7}$$

This equation can be split into two parts, each of which is a function of only one of the independent variables. Those two terms are necessarily equal to a constant, written here as $-C^2$:

$$\frac{f''}{f} + \frac{1}{y^+}\frac{f'}{f} = -\left(\frac{g''}{g} + \frac{g'^2}{g^2}\right) = -C^2. \tag{8}$$

In order to solve the differential equation in f, we have to fix the value of the function and of its derivative at one point. As long as all terms are expressed in dimensionless form, the function has to be 1 on the street centreline. The symmetry condition on this axis imposes a null derivative of the function at that point. Given those conditions, the solution of the equation is a linear combination of Bessel functions J_0 and Y_0:

$$\begin{cases} f'' + \frac{1}{y^+}f' + C^2 f = 0 \\ f(1) = 1 \\ f'(1) = 0 \end{cases} \Longrightarrow f(y^+) = \frac{J_1(C)Y_0(Cy^+) - J_0(Cy^+)Y_1(C)}{J_1(C)Y_0(C) - J_0(C)Y_1(C)}, \tag{9}$$

and is represented in Fig. 3. In order to interpret this solution physically, we can express it as a series expansion of Bessel functions, which provides an approximate solution close to the rigid boundaries:

$$\text{for } y^+ \ll 1 \begin{cases} J_0(y^+) \simeq 1 + O\left(y^{+2}\right) \\ Y_0(y^+) \simeq \frac{2}{\pi}\left[\ln\left(\frac{y^+}{2}\right) + \gamma\right] J_0(y^+) + O\left(y^{+2}\right), \end{cases} \tag{10}$$

where γ is the Euler constant, equal to 0.577.

If we then replace the Bessel functions in the equation for f (Eq. 9) by the first term in their series expansion, the velocity u^+ can be expressed as:

$$u^+(y^+, z^+) = \frac{u_*^+(z^+)}{\kappa} \ln\left(\frac{y^+}{y_i^+}\right), \tag{11a}$$

with,

$$u_*^+(z^+) = \frac{2}{\pi} \frac{g(z^+)\kappa J_1(C)}{J_1(C)Y_0(C) - J_0(C)Y_1(C)}, \tag{11b}$$

$$y_i^+ = \frac{2}{C} \exp\left[\frac{\pi}{2}\frac{Y_1(C)}{J_1(C)} - \gamma\right]. \tag{11c}$$

This result shows that the solution obtained corresponds to a classical logarithmic law for a velocity field close to a wall, and is plotted in Fig. 3. The variable y_i^+, which appears in the velocity expression, plays the same role as the dimensionless roughness parameter of the wall. By fixing the value of this roughness parameter ($y_i^+ = z_i/\delta_i$), we can determine the constant C by solving the following non-linear equation:

$$\frac{z_i}{\delta_i} = \frac{2}{C} \exp\left[\frac{\pi}{2}\frac{Y_1(C)}{J_1(C)} - \gamma\right]. \tag{12}$$

Assuming Prandtl's mixing length hypothesis, the turbulent diffusivity can be expressed as the product of a length scale and a velocity scale:

$$K = u_* \kappa y, \tag{13a}$$

which gives

$$K^+ = \frac{U_m \delta_i}{K_m} u_*^+ \kappa y^+. \tag{13b}$$

By combining this with Eq. 6 and adopting the expression for u_*^+ given in (11), we can express the constant K_m as a function of U_m in the following way:

$$K_m = \frac{2}{\pi} \frac{U_m \delta_i \kappa^2 J_1(C)}{J_1(C)Y_0(C) - J_0(C)Y_1(C)}. \tag{14}$$

The form function g, which defines the vertical profiles, is the solution of a second-order differential equation. The dimensionless form implies that the function g has to be equal to 1 at the interface, i.e., for $z = H$. The derivative g' goes to zero for $z^+ \to -\infty$, as long as the turbulent entrainment reduces for increasing distances from the interface. The solution is a decreasing exponential function:

$$\begin{cases} gg'' + g'^2 - C^2 g^2 = 0 \\ g\left(\frac{H}{\delta_i}\right) = 1 \\ g'(-\infty) = 0 \end{cases} \implies g(z^+) = \exp\left[\frac{C}{\sqrt{2}}\left(z^+ - \frac{H}{\delta_i}\right)\right]. \tag{15}$$

Function g is plotted in Fig. 4 together with the full profile obtained by the matching of Eq. 18 in Zone II, Eq. 15 in Zone I and a classical logarithmic law for the external flow. It is interesting to note that similar exponential velocity profiles for the mean flow have been found in urban (Belcher et al. 2003) and vegetation canopies (Inoue 1963; Cionco 1965; Lettau 1972). The analogy between our results, obtained in the case of a localised force on

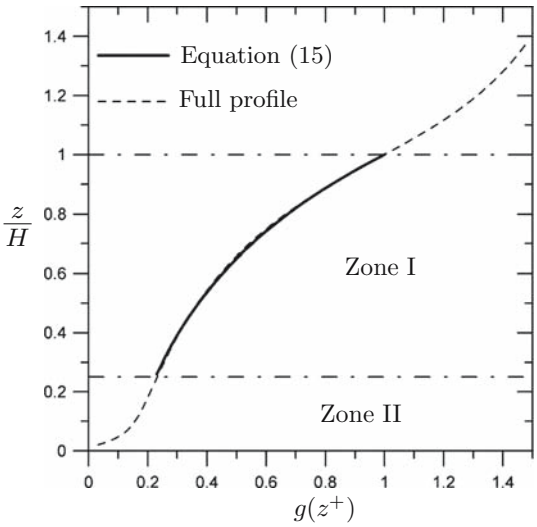

Fig. 4 Vertical profile of the dimensionless longitudinal velocity on the street axis (Zone I and Zone II are the same as in Fig. 2)

the canyon walls, and those obtained in the case of a distributed drag force within the canopy is due to the fact that these forces are both dependent on the square of the mean velocity.

Starting from the expression for g, we can determine the shear stress at the upper boundary of the street. The forcing condition requires that the magnitude of this stress has to be equal to the stress τ_H ($= \tau_0 = \rho u_*^2$) exerted by the overlying flow, which is given by:

$$\rho K_m \frac{C}{\sqrt{2}\delta_i} U_m = \rho u_*^2. \tag{16}$$

By using Eq. 14 to express K_m, this equality enables us to express U_m in terms of the friction velocity of the overlying flow:

$$U_m = u_* \sqrt{\frac{\pi}{\sqrt{2}\kappa^2 C}\left[Y_0(C) - \frac{J_0(C)Y_1(C)}{J_1(C)}\right]}. \tag{17}$$

2.1.3 Region II: Region of Influence of the Ground

We assume that the effect of the side walls has no influence on the lower part of the velocity field, close to ground level. The flow developing above the ground can then be modelled simply as a boundary layer over a rough wall, driven by an external flow:

$$\overline{u} = \frac{u_*^s}{\kappa} \ln\left(\frac{z}{z_i}\right). \tag{18}$$

The friction velocity u_*^s is determined by means of matching with the profile in the Region I at the interface between the two regions, i.e., for $z = \delta_i$. We then obtain:

$$u_*^s = U_m \frac{\kappa}{\ln\left(\frac{\delta_i}{z_i}\right)} \exp\left[\frac{C}{\sqrt{2}}\left(1 - \frac{H}{\delta_i}\right)\right]. \tag{19}$$

The solution for the velocity field (given by Eqs. 5, 15, 9 and by Eq. 18) is illustrated in Fig. 5, where velocity contours have been plotted for three different street aspect ratios ($H/W = 2$ in Fig. 5a, $H/W = 1$ in Fig. 5b, $H/W = 1/3$ in Fig. 5c).

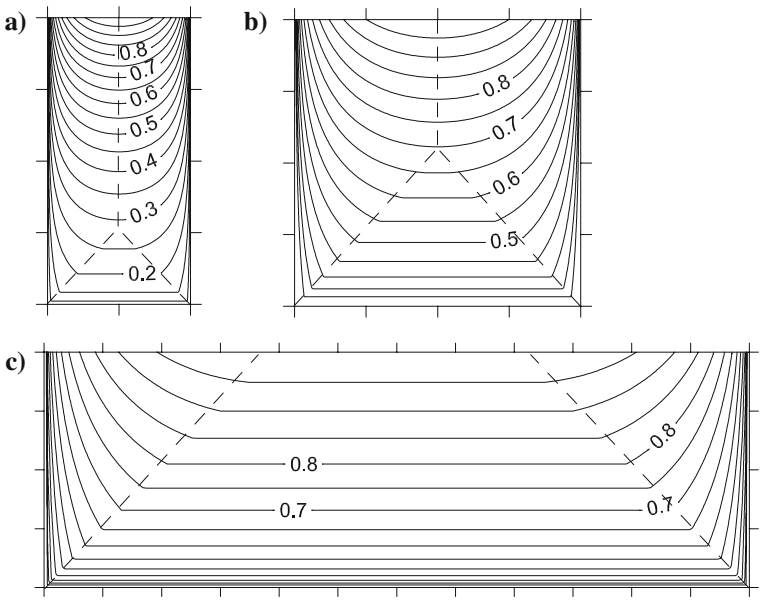

Fig. 5 Contours of dimensionless longitudinal velocity $\overline{u}/U_m$ for three different street aspect ratios: (**a**) $H/W = 1/2$, (**b**) $H/W = 1$, (**c**) $H/W = 3$

2.1.4 Mean Flow within the Street

The theoretical model provides a description of the longitudinal component of the velocity in a street whose axis is parallel to the external wind direction. The only input parameters for this model are the vertical and lateral dimensions of the street, H and W, the roughness length z_i of the street walls and the external friction velocity u_*.

For some applications it is useful to be able to compute the mean longitudinal velocity magnitude $U_{/\!/}$ within the street, defined as

$$U_{/\!/} = \frac{1}{HW}\int_0^H \int_{-W/2}^{W/2} \overline{u} dy dz. \tag{20}$$

It can be shown that the mean velocity is given by

$$U_{/\!/} = U_m \frac{\delta_i^2}{HW}\left[\frac{2\sqrt{2}}{C}(1-\beta)\left(1-\frac{\pi}{2}H_1(C)\right)+\beta\frac{2\alpha-3}{\alpha}+\left(\frac{W}{\delta_i}-2\right)\frac{\alpha-1}{\alpha}\right], \tag{21a}$$

with

$$\alpha = \ln\left(\frac{\delta_i}{z_i}\right), \tag{21b}$$

$$\beta = \exp\left[\frac{C}{\sqrt{2}}\left(1-\frac{H}{\delta_i}\right)\right], \tag{21c}$$

where U_m is defined by Eq. (17), C by Eq. (11) and H_1 is a first-order Struve function. A detailed derivation of Eq. (21) is provided in Appendix 1. The function $H_1(C)$ can be

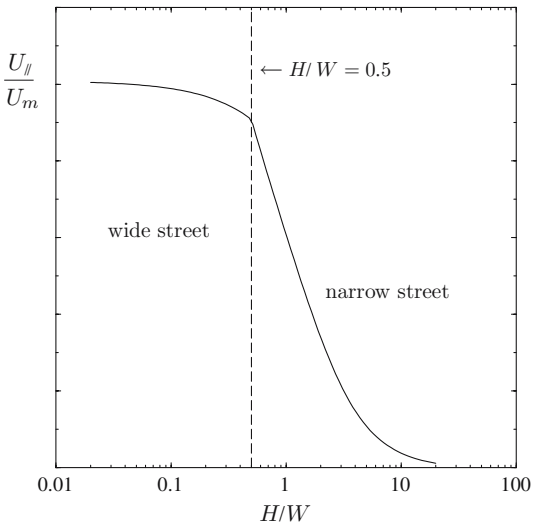

Fig. 6 Dimensionless longitudinal mean velocity plotted as a function of street aspect ratio for $z_i = 0.01\,\mathrm{m}$ and $H = 20\,\mathrm{m}$

approximated with an error that does not exceed 0.2 % by a polynomial expansion of the form (Abramowitz and Stegun 1965):

$$\frac{\pi}{2} H_1(C) \simeq \frac{C^2}{1^2 \times 3} - \frac{C^4}{1^2 \times 3^2 \times 5} + O(C^6). \tag{22}$$

For this expansion to be valid C must be positive and smaller than 1; in this particular case, it is evident from Eq. 12 that C has to be positive. Equation 12 also enables us to provide a numerical bound on the physical likely values of C: as long as the dimensionless roughness length z_i/δ_i cannot reasonably exceed a value of 0.01 (that means that, for a characteristic length scale of the street $\delta \approx 10$ m, we obtain a maximum roughness length $z_i \approx 0.1\,\mathrm{m}$), from Eq. 12 it can be inferred that C has to be smaller than 0.716.

The dimensionless mean longitudinal velocity $U_{/\!/}/U_m$ has been plotted in Fig. 6 as a function of H/W, and this clearly shows the transition from a wide street to a narrow street, for $H/W \approx 0.5$. The dimensionless mean velocity in a wide street is almost independent of the aspect ratio, whereas the dimensionless mean velocity in a narrow street is strongly dependent on the aspect ratio. So for wide streets, the cross-sectionally averaged velocity leads to a constant value, and the mass flux in the street is simply proportional to the cross-sectional area of the street.

2.2 Numerical Simulations

In order to verify the model, we have compared its results with numerical simulations performed using the code MERCURE (Carissimo et al. 1995). MERCURE is a three-dimensional numerical code that implements a finite difference method to solve the Reynolds-Averaged Navier–Stokes equations. For this study, a standard k-ε turbulence model was used, with a non-regular mesh and the size of the grid cell close to the rigid boundaries was set equal to $H/40$. Seven street geometry configurations have been tested, corresponding to a different street aspect ratio H/W: 1/4, 1/3, 1/2, 1, 2, 3 and 4, where H was taken constant and equal to 20 m. The roughness lengths of the roof and of the side wall of the street have been set equal to 50 mm. In order to define a solution independent of the initial conditions and of the

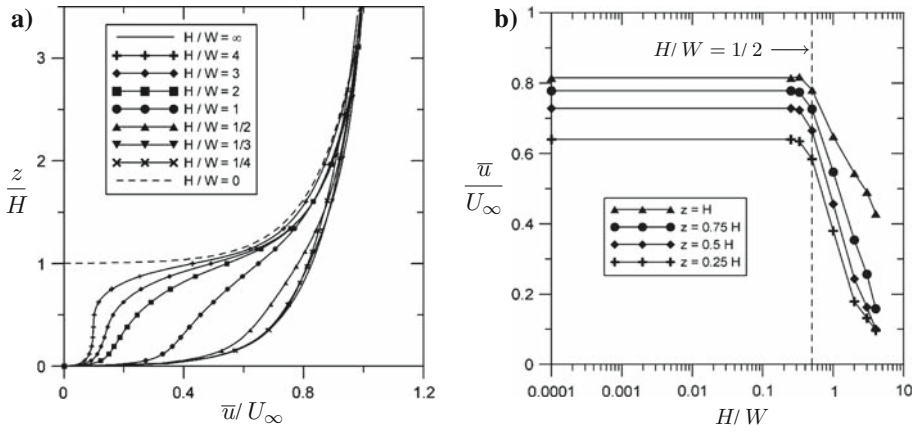

Fig. 7 Evolution of the longitudinal mean velocity within the street for varying street aspect ratios H/W. (**a**) Vertical mean velocity profiles at the street centre for different aspect ratios H/W; (**b**) Flow regimes for a wind parallel to the street axis: influence of the street aspect ratio on the longitudinal velocity on the street axis ($y = \delta_i$), for different heights

longitudinal coordinate x, the flow was defined to be periodic in the x-direction (i.e., the flow at the downstream end of the simulation was identical to the injected flow at the upstream entry to the section).

The mean velocity profiles within the street for different street aspect ratios are presented in Fig. 7a. The different profiles are bounded by the profiles corresponding to the limiting cases $H/W \to 0$ and $H/W \to \infty$. In the case $H/W \to 0$, the distance between the lateral walls tends to infinity and the velocity field is that of a turbulent boundary layer developing on a rough wall. In the case given by the limit $H/W \to \infty$, the lateral walls are close together and the resulting flow field is given by a turbulent boundary layer displaced above the building roofs. Between these two limiting configurations, the flow within the street varies depending on the resistance exerted by the side walls. As expected, the mean velocity within the street is reduced for increasing values of the ratio H/W.

2.2.1 Flow Regimes

In order to verify the existence of two flow regimes, we plotted the dependence of the velocity component on the street aspect ratio H/W (Fig. 7b). This confirms quite clearly that there are two different flow regimes, depending on the street aspect ratio. For small values of H/W ($H/W \leq 0.5$), the velocity at the centre of the street is independent of H/W and equal to the value for the limiting case $H/W \to 0$. This means that the flow within the street is independent of the side walls and behaves as a boundary layer developing above ground level. However once H/W exceeds a critical value ($H/W \geq 0.5$) the side walls begin to have a significant influence on the flow, and the centreline velocity decreases as H/W increases, because of the drag from the side walls.

2.2.2 Comparison with the Theoretical Model

In order to validate the theoretical model, we have compared the velocity profiles computed by MERCURE with those given by the model. Here we will focus on two configurations in

particular ($H/W = 1$ and $H/W = 2$), which are characteristic of many real street geometries. Both of these correspond to the narrow street regime.

The vertical profiles on the street axis obtained from the numerical simulations are presented in Fig. 8a, b together with the theoretical profiles computed using Eqs. 15 and 18. The parameter C was calculated from Eq. 12, using the values of H, W and z_0 appropriate for each configuration. The value of U_m used to calculate the profiles was obtained by matching the model velocity at height $z = H$ to that computed by the numerical simulation at that height. For both configurations presented here, there is good agreement between the theoretical model and the numerical results. This agreement confirms the validity of the modelling assumption that the domain can be divided into two regions, corresponding to regions of influence of the floor and the side walls, and that the boundary between these regions depends on the aspect ratio H/W.

In a similar way, the horizontal profile of the axial velocity component $\overline{u}$ have been plotted in Fig. 8c, d, for the two configurations. The profiles have been normalized by means of the velocity at the centre of the street for each level. Except for the profile at the interface ($z/H = 1$), the different numerical profiles appear to be self-similar, which is a result that justifies the use of the method of the separation of variables. The profiles are in good agreement with the theoretical curve given by Eq. 9. This agreement fails close to the interface between the street and the external flow because, at that level, the influence of the external flow on flow dynamics has to be taken into account and cannot be considered only dependent on the effect of the side walls.

In order to compare the turbulent characteristics of the flow in Region I, the turbulent diffusivity profiles calculated using the numerical code MERCURE and the theoretical model for Region I have been plotted in the Fig. 8e, f. The two sets of results agree well, but throughout Region I and above it.

3 Wind with any Orientation

As already mentioned, several studies are available in the literature for flow within a street whose axis is perpendicular to the wind direction, but there are relatively few that consider the flow induced in a street by an external wind blowing at an arbitrary angle to the street axis. In the previous section the specific case of a wind parallel to the street axis was discussed. In this section we will now consider how that result can be generalized to the case of a wind blowing at an arbitrary orientation relative to the street axis. In the introduction it was mentioned that this configuration leads to a three-dimensional flow characterized by helicoidal streamlines. Up until now, it has generally been assumed that this flow can be modelled by a superposition of the two asymptotic solutions for flow parallel to the street and flow perpendicular to the street. But this assumption neglects any possible non-linear interaction between the two flow fields, which would invalidate their combination by superposition. As far as we are aware, there is no previous study of the nature of such a non-linear interaction. The aim of this section is therefore to investigate whether the flow generated in a street by wind at arbitrary orientation can be modelled by linear superposition of the two asymptotic cases.

As before, we consider an infinitely long, two-dimensional symmetrical street except that it will now be more convenient to locate the origin of the y-axis at the centre of the street (i.e., the street occupies now the region $-W/2 \leq y \leq W/2$, $0 \leq z \leq H$). The x, y and z coordinate system is defined as in Fig. 1. The external mean flow is assumed to form an angle θ_∞ with respect to the street axis (so $\theta_\infty = 0°$ for wind direction parallel to the street axis

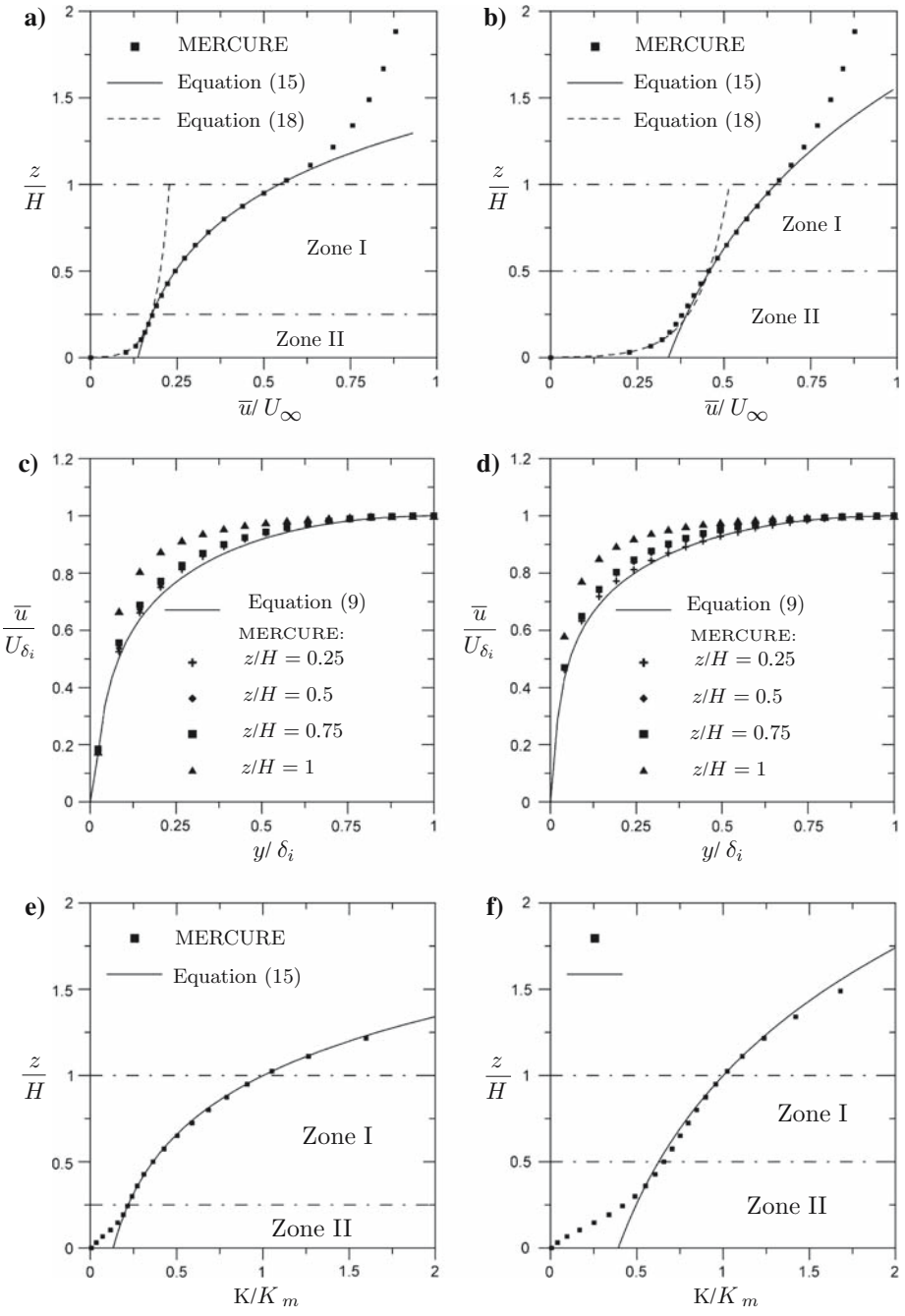

Fig. 8 Wind parallel to the street axis: comparison between theoretical model and MERCURE numerical simulations. (**a**) Vertical profile of horizontal velocity on the street axis for an aspect ratio $H/W = 2$. (**b**) Same as (**a**) for an aspect ratio $H/W = 1$. (**c**) Horizontal profile of horizontal velocity within a street for an aspect ratio $H/W = 2$. (**d**) Same as (**c**) for an aspect ratio $H/W = 1$. (**e**) Vertical profile of turbulent diffusivity vertical profile on a street axis for an aspect ratio $H/W = 2$. (**f**) Same as (**e**) for an aspect ratio $H/W = 1$

and $\theta_\infty = 90°$ for a perpendicular direction). The longitudinal and the transverse velocity components are referred to as U_∞ and V_∞, from which $V_\infty/U_\infty = \tan(\theta_\infty)$ (see Fig. 1).

3.1 Theoretical Analysis

Generally, the turbulent flow can be described by the averaged Navier–Stokes equations, neglecting viscous effects:

$$\frac{\partial \overline{u_i}}{\partial t} + \overline{u_j}\frac{\partial \overline{u_i}}{\partial x_j} = -\frac{1}{\rho}\frac{\partial P}{\partial x_i} - \frac{\partial \overline{u_i' u_j'}}{\partial x_j}. \tag{23}$$

We assume that the external flow is stationary and that the street has an infinite length in the x direction, so that all variables (except for the pressure) do not vary in the x direction, i.e. all terms containing $\partial/\partial x$ and $\partial/\partial t$ in Eq. 23 are equal to zero. As already assumed in the case of a wind parallel to the street axis, the longitudinal pressure gradient can be neglected compared with the Reynolds stress terms, because the flow is driven by wind shear, not by the pressure gradient. Given these assumptions, the momentum equations can be written as:

$$\boxed{\overline{v}\frac{\partial \overline{u}}{\partial y} + \overline{w}\frac{\partial \overline{u}}{\partial z}} = -\frac{\partial \overline{u'v'}}{\partial y} - \frac{\partial \overline{u'w'}}{\partial z}, \tag{24}$$

$$\overline{v}\frac{\partial \overline{v}}{\partial y} + \overline{w}\frac{\partial \overline{v}}{\partial z} = -\frac{1}{\rho}\frac{\partial P}{\partial y} - \frac{\partial \overline{v'^2}}{\partial y} - \frac{\partial \overline{v'w'}}{\partial z}, \tag{25}$$

$$\overline{v}\frac{\partial \overline{w}}{\partial y} + \overline{w}\frac{\partial \overline{w}}{\partial z} = -\frac{1}{\rho}\frac{\partial P}{\partial z} - \frac{\partial \overline{v'w'}}{\partial y} - \frac{\partial \overline{w'^2}}{\partial z}. \tag{26}$$

In the particular case of an external wind parallel to the street axis, these equations reduce to Eq. 2. In the particular case of an external wind perpendicular to the street axis, the flow dynamics are described by means of Eqs. 25 and 26. The analysis of these different equations yields a better understanding of the coupling between the longitudinal and transverse components of the flow. It is worth noting that Eqs. 25 and 26 describe the flow as if it were driven by an external velocity component V_∞, oriented perpendicularly to the street axis. This means that the transverse component (in the plane y–z) of the helicoidal flow is identical to the mean flow induced by a perpendicular wind direction, as described in the literature. That is, the transverse component of the flow is entirely independent of any longitudinal component of the flow. On the other hand, Eq. 24, which describes the longitudinal component of the helicoidal flow, differs from Eq. 2, which was derived in the case of an external wind parallel to the street axis, because it contains two additional terms (the terms in the box) which represent the transfer of momentum for the transverse flow to the longitudinal flow. In this sense, the coupling between the two flows is therefore a one-way coupling.

The evolution of the transverse component can be considered to be independent of the longitudinal one; on the other hand, compared with the asymptotic case of a parallel wind, the presence of the transverse component modifies the longitudinal component of the flow. The role of the terms in the box of Eq. 24 should be to homogenise the velocity distribution on the cross-section of the street (Dobre et al. 2005). This means that the helicoidal flow cannot be modelled as a superposition of the two components and that the analytical model described in Sect. 2 cannot therefore be generalized. In principle, it will be necessary to modify the model for the longitudinal component, to take account of the contribution from the transverse velocity. Nevertheless, the integral form of Eq. 25 would not be different from

Eq. 2, for the case of an external wind aligned with the street axis. In this case both equations reduce to

$$\int\int_S \vec{\vec{\tau}} \cdot \vec{n} dS = 0,$$

where $\vec{\vec{\tau}}$ represents the Reynolds stress tensor, $\vec{n}$ the normal to the wall and S the integration surface. From a physical point of view this shows that the terms in the box in Eq. 25 do not influence the spatially-averaged momentum flux along the street axis and that their effect is related only to the velocity distribution within the street. Here, we propose a simplified model for the spatially-averaged mean flow in the longitudinal direction

$$U_{\text{street}}(\Theta_\infty) = \frac{1}{HW} \int_0^H \int_{-W/2}^{W/2} \overline{u} dy dz, \tag{27}$$

based on the assumption that the additional terms in Eq. 24 will modify the spatial distribution of the longitudinal velocity in the street, but not the spatially-averaged value of that velocity. In other words, the spatially-averaged longitudinal velocity U_{street} will still only depend on the component of the external velocity parallel to the street axis (U_∞). It then follows that the model developed previously can be used to compute U_{street}:

$$U_{\text{street}}(\Theta_\infty = 0°) = U_{/\!/}, \tag{28}$$

where $U_{/\!/}$ is defined by Eq. 21 and calculated from the velocity component U_∞. It is worth noting that U_{street} has to be proportional to $\cos(\theta_\infty)$. The model has been tested by comparing it with the results of numerical simulations; this is described in detail in Sect. 3.2.

The nature of the coupling between the two flow components provides a way of characterizing the helicoidal flow within the street. If Eq. 28 is correct, it can be expected that δs, the step of the helix, will be proportional to $\cot(\theta_\infty)$: this implies that δs tends to zero as the wind becomes perpendicular to the street axis and that it tends to infinity as the wind becomes parallel to the street orientation. We also need to consider that, although the helix is periodic along the street axis, the angle of the streamlines changes with height because the velocity on the street centreline is different at the top and at the bottom of the street. Close to the ground, the transverse component of the velocity $\overline{v}$ diminishes more rapidly than $\overline{u}$, the longitudinal component. A reduction in the absolute value of the angle θ should then be observed close to the ground, and hence $|\theta_{\text{ground}}| < \theta_H < \theta_\infty$. This result confirms the field observations of Nakamura and Oke (1988) in a street of Kyoto.

3.2 Numerical Model of an Infinite Two-dimensional Street

In order to verify the assumptions described in the previous paragraph, numerical simulations were performed using the MERCURE code, for a symmetrical street with an aspect ratio $H/W = 1$. Several values of θ_∞ have been tested: 0, 15, 30, 45, 60, 75, and 90°.

3.2.1 Flow Topology

Except for the case $\theta = 0°$ (wind parallel to the street axis), the flow topology within the street is characterized by an irregular helix, as shown in Fig. 9—the wind direction is closer to the axis of the street at the bottom of the street than it is at the top, and is due to the channelling effect of the street, which increases close to the ground. This phenomenon is confirmed by the analysis at different heights of the wind orientation on the horizontal plane

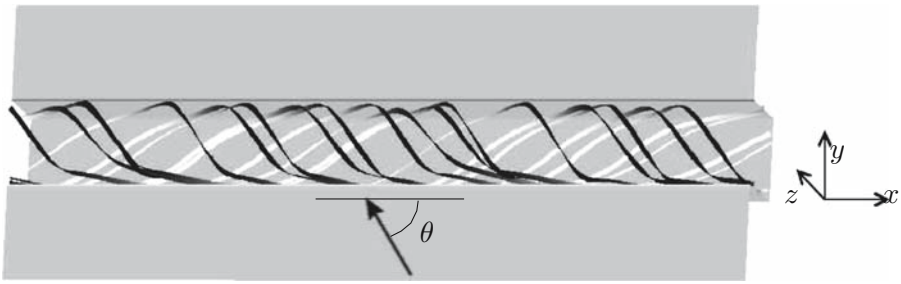

Fig. 9 Flow topology simulated using the MERCURE code representing a three-dimensional view of the helicoidal flow within the street in the case of $\theta = 60°$. The black stripes correspond to the streamlines in the upper part of the flow and the white stripes to the streamlines close to the ground

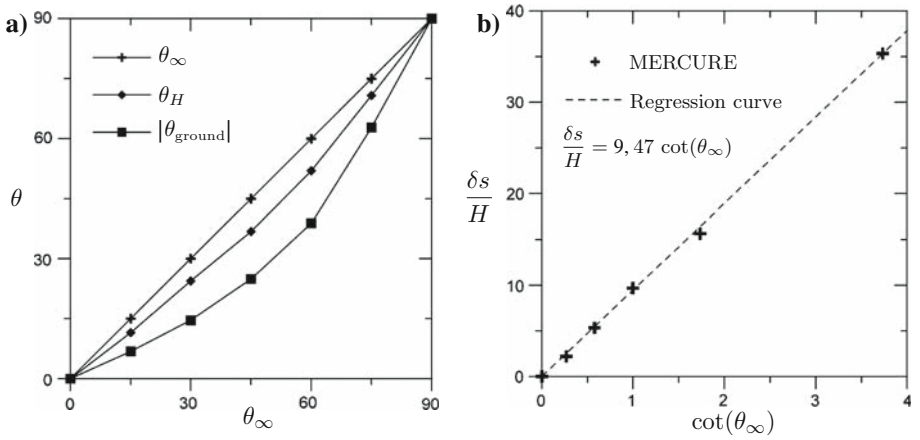

Fig. 10 Characteristics of the flow given by the numerical simulations using the MERCURE code. (**a**) Flow deviation: wind orientation at roof level and at ground level for different angles of the external flow. (**b**) Helicoid step δs as a function of wind orientation: evidence of the linear relation $\delta s \propto \cot(\theta_\infty)$

(Fig. 10a): the angle between the mean velocity direction and the street axis becomes smaller and smaller as the ground level is approached. This effect reaches a maximum for $\theta_\infty = 45°$, consistent with the field measurements obtained by Nakamura and Oke (1988).

In Fig. 10b, the helix step δs is plotted as a function of $\cot(\theta_\infty)$: the relation between the two is linear. Although the angle of the streamlines in the helix depends on the vertical distance from the bottom of the street, the step length δs is constant through the street. It is interesting to notice that, for an angle $\theta_\infty < 45°$, δs is about 20 times the street height, implying that the helicoidal flow appears only if the street is sufficiently long. There are many practical situations where this condition is not satisfied—the ratio of the street length to the street height is typically of the order of 5—and helicoidal flow may not appear.

3.2.2 Transversal Component

The velocity profiles in the y–z plane, normalized with V_∞ as the reference velocity component, are plotted in Fig. 11a. For any wind direction, the profiles collapse onto a single curve. The transverse component $\overline{w}$ at mid-height exhibits the same behaviour. This confirms the assumption that there is no coupling between the two components $\overline{v}$ and $\overline{w}$ and the component

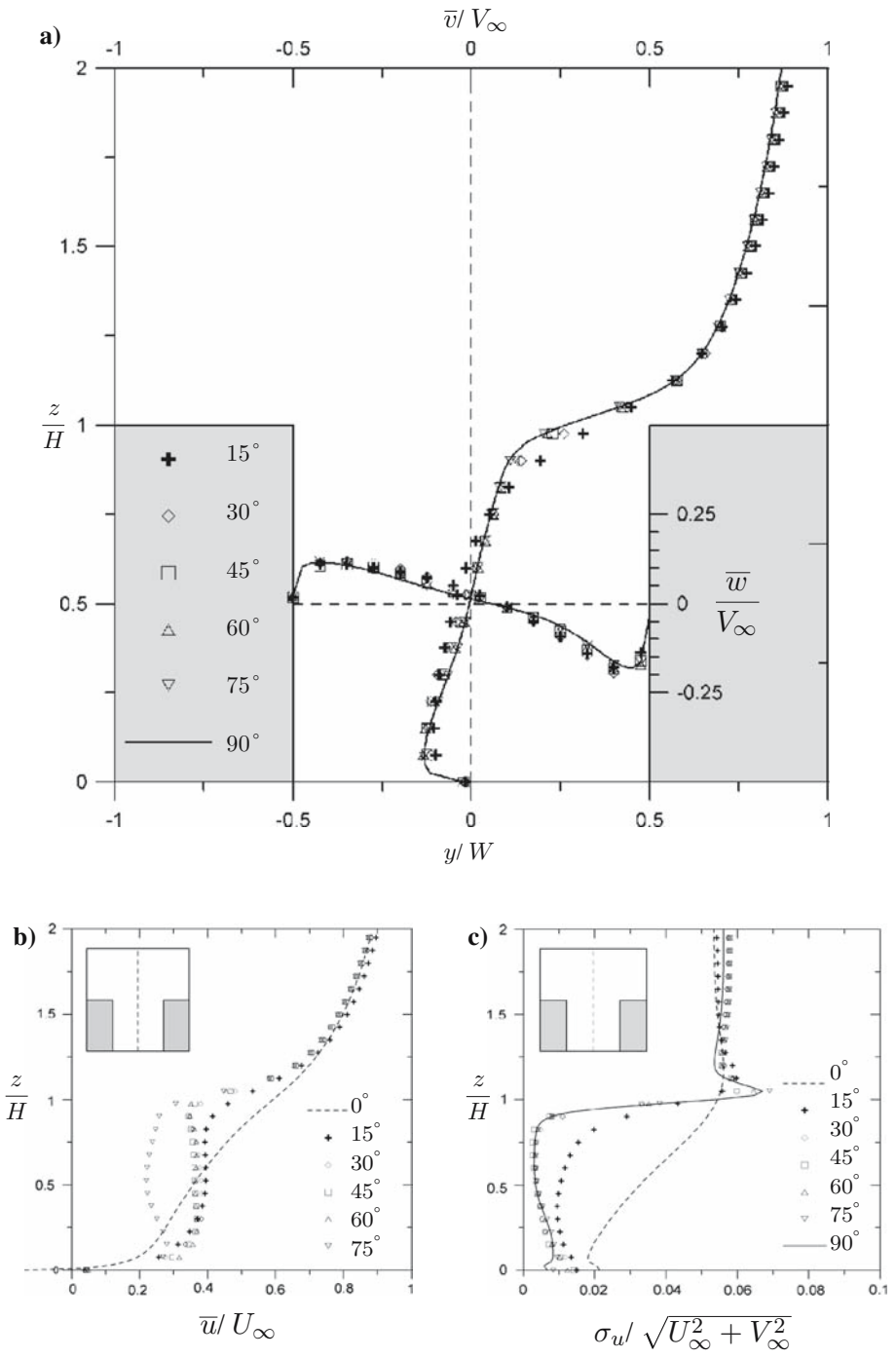

Fig. 11 Flow within the street for different external wind directions: mean velocity and velocity fluctuations (numerical simulations performed with the MERCURE code). (**a**) Velocity on the horizontal plane y–z. (**b**) Longitudinal velocity. (**c**) Velocity fluctuation

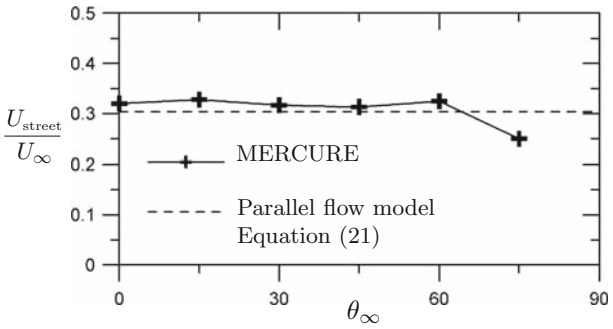

Fig. 12 Mean longitudinal velocity component in a section of the street

$\overline{u}$. Therefore, for any wind direction, the mean flow in the y–z plane is identical to that for a flow driven by an external wind that is perpendicular to the street axis.

3.2.3 Longitudinal Component

The longitudinal velocity profiles on the street axis are shown in Fig. 11b. There is a clear difference between the flow behaviour for a wind parallel to the street axis ($\theta_\infty = 0°$) and all other wind orientations $\theta_\infty \neq 0°$. In the first case, the profile corresponds to the model described in Sect. 2. For all other angles, the mean velocity is much more uniform within the street. This is caused by the coupling term in Eq. 24, which tends to homogenize the velocity component $\overline{u}$, as predicted. Furthermore, for $15° \leqslant \theta_\infty \leqslant 60°$, the velocity profiles $\overline{u}/U_\infty$ can be superposed on each other (for $\theta_\infty = 75°$, the velocity becomes weaker compared to the other cases). Apart from these cases, then, the longitudinal velocities in the cavity $\overline{u}$ scale on the parallel component of the external wind, U_∞.

Based on the above hypothesis, the dependence of the spatially-averaged mean velocity component U_{street} on U_∞ can be evaluated for varying values of θ_∞, in order to test whether it can be modelled using the analytical model for the case of a parallel wind. In Fig. 12 the evolution of U_{street} is shown as a function of the wind direction, calculated by means of numerical simulations. It can be observed that $U_{\text{street}}/U_\infty$ is almost independent of the external wind direction. However, as θ_∞ approaches 90°, this is no longer true, which is certainly due to the fact that, for that angle, both U_{street} and U_∞ go to zero. The relation between these two velocities then becomes more difficult to predict, and the ratio between the two differs from the predicted value. It can be seen that, for $\theta_\infty = 0°$, the ratio $U_{\text{street}}/U_\infty$ is close to the value obtained for all the other wind directions, even though the velocity profile is really quite different. This justifies the assumption adopted in the proposed model and allows us to use it to determine the mean velocity within the street for any orientation of the external wind. To test this model, we have used Eq. 21 to evaluate the spatially-averaged mean velocity on a section of the street. The constant value obtained by means of this method shows good agreement with the values using numerical simulations based on the MERCURE code.

3.2.4 Turbulence

The evolution of the velocity fluctuations (calculated from the kinetic energy k, using the relation $\sqrt{2k/3}$, assuming an isotropic turbulence) is shown in Fig. 11c. It can be observed

that, for $\theta_\infty \geqslant 30°$, the intensity of the turbulence does not depend on the external wind direction and that the profiles superimpose relatively well. For smaller values of the angle θ, the turbulence intensity takes higher values. The greater turbulence intensity may be due to the entrainment within the street of large-scale vortices from the external flow, as its mean component is parallel to the street axis. Finally it is worth noting that, at the interface level, the turbulence intensity is independent of the external wind direction, which is in agreement with the experimental results of Rotach (1995).

3.2.5 Influence of Street Aspect Ratio

The comparison between theoretical and analytical results presented here concerns only a single street geometry, for which $H/W = 1$. It is likely that some of the results obtained here would be different for other aspect ratios. In particular, we would expect a quite different flow behaviour in the case of a wider street, passing from the skimming flow to the wake interference flow regime. In this case the mixing properties of the flow change substantially (Harman et al. 2004) and the velocity field within the street exhibits a stronger coupling with the overlying boundary-layer flow (Salizzoni 2006). Conversely, as the street aspect ratio H/W increases, the presence of a second counter-rotating cell in the lower part of the street would radically alter the mean velocity profile. Further work is therefore required to fully define the applicability of this simple model.

4 Conclusions

In this study, we have examined the flow within a street canyon driven by an external wind with arbitrary direction relative to the street axis. We developed a theoretical model for the flow in a street driven by an external wind parallel to the street axis. The domain within the street was divided into two different regions, with dynamics influenced mainly by the ground or by the side walls, and from this we derived two different flow regimes, generating two different velocity profiles. The model agrees well with the results obtained using detailed numerical simulations obtained with the Reynolds-Averaged Navier–Stokes code MERCURE.

We then considered the influence of wind direction. In particular, we have shown that certain aspects of the flow can be obtained from the linear superposition of two asymptotic cases: flow parallel to the street and flow perpendicular to the street. This confirms an assumption already made by other workers. However, not all features of the flow can be modelled by such a linear superimposition of asymptotic cases. Using numerical simulations of the flow generated by an external wind at different orientation, we showed that the flow within the street is determined by a coupling between the longitudinal and the transverse components of the flow. This is a one-way coupling—the longitudinal component is influenced by the transverse component, whereas the transverse component is not affected by the longitudinal component. It was also shown that the mean longitudinal velocity, averaged over a street section, is directly proportional to the cosine of the angle of incidence, for any wind orientation. This implies that the velocity component can be evaluated from the model for a wind parallel to the street.

The results from this study will allow a more detailed and improved modelling of the flow and dispersion of pollutants within street canyons. They also provide a useful basis for the investigation and the modelling of flow and dispersion at street intersections, where the transfer phenomena are determined by the flows entering and leaving different streets.

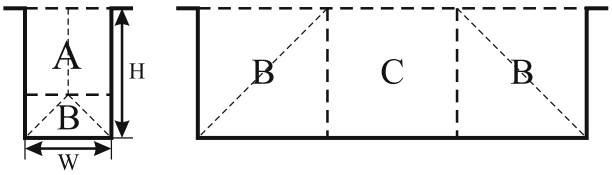

Fig. 13 Definition of Region A, B and C for the spatial integration of the velocity profile

5 Appendix 1: Derivation of Eq. 21

We define $\delta = min(H, W/2)$. Regions A, B and C are defined in Fig. 13.

5.1 Region A

We assume a velocity profile of the form

$$u(z, y) = U_m f\left(\frac{y}{\delta}\right) g\left(\frac{z}{\delta}\right), \tag{29}$$

$$\text{with} \begin{cases} f(y^+) = \dfrac{J_1(C)Y_0(Cy^+) - J_0(Cy^+)Y_1(C)}{J_1(C)Y_0(C) - J_0(C)Y_1(C)} \\ \\ g(z^+) = \exp\left(\frac{Cz^+}{\sqrt{2}}\right). \end{cases}$$

C is obtained by the following equation (earlier Eq. 12)

$$\frac{z_i}{\delta_i} = \frac{2}{C}\exp\left[\frac{\pi}{2}\frac{Y_1(C)}{J_1(C)} - \gamma\right],$$

where z_0 is the roughness length of the wall.
The air flux in the Region A can be computed as

$$Q_1 = 2\int_0^{\delta_i}\int_{-H+\delta_i}^{0} u(y, z)dzdy = 2U_m\delta_i^2\int_0^1 f\left(y^+\right)dy^+\int_{1-H/\delta_i}^{0} g\left(z^+\right)dz^+,$$

and it can be shown that

$$\int_0^1 f(y^+)dy^+ = \int_0^1 \frac{J_1(C)Y_0(Cy^+) - J_0(Cy^+)Y_1(C)}{J_1(C)Y_0(C) - J_0(C)Y_1(C)}dy^+ = 1 - \frac{\pi}{2}H_1(C),$$

$H_1(C)$ being the first-order Struve function. In the case that $C \leq 1$, we have (Abramowitz and Stegun 1965):

$$\frac{\pi}{2}H_1(C) \simeq \frac{C^2}{1^2 \times 3} - \frac{C^4}{1^2 \times 3^2 \times 5} + O(C^6),$$

with an error of 0.2% (Eq. 22 earlier).
It can be also shown that

$$\int_0^1 g(z^+)dz^+ = \frac{\sqrt{2}}{C}\left\{1 - \exp\left[\frac{C}{\sqrt{2}}\left(1 - \frac{H}{\delta_i}\right)\right]\right\},$$

then we obtain

$$\Rightarrow Q_1 = U_H\delta_i^2\frac{2\sqrt{2}}{C}(1-\beta)\left(1 - \frac{\pi}{2}H_1(C)\right).$$

It can be observed that, if $W/2 > H \Rightarrow \delta = H \Rightarrow \beta = 1 \Rightarrow Q_1 = 0$.

5.2 Region B

We assume a velocity profile of the form

$$u(y,z) = U_{\delta_i} \frac{\ln\left(\frac{d}{z_i}\right)}{\ln\left(\frac{\delta_i}{z_i}\right)}, \tag{30}$$

where d is the distance from the nearest wall and

$$U_{\delta_i} = U_m \exp\left(\frac{C}{\sqrt{2}}\left(1 - \frac{H}{\delta_i}\right)\right) = \beta U_m.$$

Equation 30 is an approximated form of the exact solution (Eq. 9), which is used to allow an analytical integration of the velocity. From Fig. 3, we observe that this assumption does not induce an error exceeding a few percent. Then, the air flux in the Region B can then be computed as

$$Q_2 = 4\int_{y=0}^{y=\delta_i}\int_{z=0}^{z=y} u(y,z)dydz = \frac{4\beta U_m}{\ln\left(\frac{\delta_i}{z_i}\right)}\int_{y=0}^{y=\delta_i}\int_{z=0}^{z=y} \ln\left(\frac{z}{z_i}\right)dydz,$$

$$Q_2 = \frac{4\beta U_m}{\ln\left(\frac{\delta_i}{z_i}\right)}\int_{y=0}^{y=\delta_i}\left[y\ln\left(\frac{y}{z_i}\right) - y\right]dy,$$

$$Q_2 = \beta U_H \delta_i^2 \frac{2\ln\left(\frac{\delta_i}{z_i}\right) - 3}{\ln\left(\frac{\delta_i}{z_i}\right)} = U_m \delta_i^2 \beta \frac{2\alpha - 3}{\alpha},$$

with $\alpha = \ln\left(\frac{\delta_i}{z_i}\right)$.

5.3 Region C

We assume a velocity profile of the form

$$u(y,z) = U_m \frac{\ln\left(\frac{z}{z_i}\right)}{\ln\left(\frac{\delta_i}{z_i}\right)}. \tag{31}$$

The air flux in the Region C can then be computed as

$$Q_3 = (W - 2H)\int_0^{\delta} u(y,z)dy = U_m \delta_i^2 \left(\frac{W}{\delta_i} - 2\right)\left(\frac{\alpha - 1}{\alpha}\right).$$

We observe that, if $W/2 < H \Rightarrow \delta = W/2$ and we have that $Q_3 = 0$.

5.4 Spatially-averaged Velocity in the Cross-section of the Street

As long as

$$U_{\text{rue}} = \frac{Q_1 + Q_2 + Q_3}{HW},$$

we obtain finally Eq. 21

$$U_{/\!/} = U_m \frac{\delta_i^2}{HW} \left[\frac{2\sqrt{2}}{C}(1-\beta)\left(1 - \frac{\pi}{2} H_1(C)\right) + \beta \frac{2\alpha - 3}{\alpha} + \left(\frac{W}{\delta_i} - 2\right) \frac{\alpha - 1}{\alpha} \right].$$

References

Abramowitz M, Stegun IA (1965) Handbook of mathematical functions. Dover Pubs., New York, 1046 pp

Albrecht F (1933) Untersuchungen der vertikalen Luftzirkulation in der Grossstadt. Met Zt 50:93–98

Baranger P (1986) Influence des conditions microclimatologiques sur la pollution d'une rue. PhD thesis, Université de Toulouse

Belcher S, Jerram N, Hunt J (2003) Adjustment of a turbulent boundary layer to a canopy of roughness elements. J Fluid Mech 488:369–398

Berkowicz R, Hertel O, Sorensen NN, Michelsen JA (1994) Modelling air pollution from traffic in urban areas. In: Perkins RJ, Beleher BE (eds) IMA conference on flow and dispersion through groups of obstacles, pp. 121–141

Berkowicz R, Palmgren F, Hertel O, Vignati E (1996) Using measurements of air pollution in streets for evaluation of urban air quality–meteorological analysis and model calculations. Sci Total Environ 189/190:259–265

Bottema M (1997) Turbulence closure model 'constants' and the problems of 'inactive' atmospheric turbulence. J Wind Eng Ind Aero 67–68:897–908

Ca VT, Aseda T, Armfield S (1995) Characteristics of wind field in a street canyon. J Wind Eng Ind Aero 57(1):63–80

Carissimo B, Dupont E, Musson–Genon L, Marchand O (1995) Note de principe du code MERCURE version 3.1. EDF-DER, HE-3395007B

Cheng H, Castro IP (2002) Near wall flow over urban-like roughness. Boundary-Layer Meteorol 104:229–259

Cionco R (1965) A mathematical model for air flow in a vegetative canopy. J Appl Meteorol 4:517–522

Dabberdt WF, Hoydysh WG (1991) Street canyon dispersion: sensitivity to block shape and entrainment. Atmos Environ 25(7):1143–1153

Dobre A, Arnold S, Smalley R, Boddy J, Barlow J, Tomlin A, Belcher J (2005) Flow field measurements in the proximity of an urban intersection in London, UK. Atmos Environ 39:4647–4657

Eerens HC, Sliggers CJ, Van den Hout KD (1993) The CAR model : the Dutch method to determine city street air quality. Atmos Environ 27(4):389–399

Grimmond CSB, Oke TR (1999) Aerodynamic properties of urban areas derived from analysis of surface form. J Appl Meteorol 38:1262–1292

Harman IN, Barlow J, Belcher SE (2004) Scalar fluxes from urban street canyons. Part II: model. Boundary-Layer Meteorol 113:387–409

Hassan AA, Crowther JM (1998) Modelling of fluid flow and pollutant dispersion in a street canyon. Environ Monit Assess 52(1–2):281–297

Hertel O, Berkowicz R (1989) Modelling pollution from traffic in a street canyon. Evaluation of data and model developement. Technical report, DMU Luft A-129, NERI

Hoydysh WG, Dabberdt WF (1988) Kinematics and dispersion characteristics of flows in asymetric street canyons. Atmos Environ 22(12):2677–2689

Hussain M, Lee BE (1980) An investigation of wind forces on three dimensional roughness elements in a simulated atmospheric boundary layer flow. Part II : flow over large arrays of identical roughness elements and the effect of frontal and side aspect ratio variations. Technical report, Dept. of Build. Sce, Univ. of Sheffield, pp. 1–81

Inoue E (1963) On the turbulent structure of air flow within crop canopies. J Meteorol Soc Jap Ser 41(11):317–326

Johnson GT, Hunter LJ (1995) A numerical study of dispersion of passive scalars in city canyons. Boundary-Layer Meteorol 75:235–262

Johnson WB, Ludwig FL, Dabberdt WF, Allen RJ (1973) An urban diffusion simulation model for carbon monoxide. J Air Pollut Control Assoc 23:490–498

Lettau HH (1972) Class notes (unpublished) from Meteorology 403, Micrometeorology, at the University of Wisconsin, Madison.

MacDonald RW (2000) Modelling the mean velocity profile in the urban canopy layer. Boundary-Layer Meteorol 97:25–45

MacDonald RW, Carter S, Slawson PR (2000) Measurements of mean velocity and turbulence statistics in simple obstacle arrays at 1:200 scale. Technical report, University of Waterloo, Department of Mechanical Engineering, pp. 1–100

MacDonald RW, Griffiths RF, Hall DJ (1998) A comparison of results from scaled field and wind tunnel modelling of dispersion in arrays of obstacles. Atmos Environ 32(22):3845–3862

Nakamura Y, Oke T (1988) Wind, temperature and stability conditions in an east-west oriented urban canyon. Atmos Environ 22(12):2691–2700

Oke TR (1988) Street design and urban canopy layer climate. Energy Buildings 11:103–113

Rafailidis S (1997) Influence of building areal density and roof shape on the wind characteristics above a town. Boundary-Layer Meteorol 85:255–271

Raupach MR, Thom AS, Edwards I (1980) A wind-tunnel study of turbulent flow close to regularly arrayed rough surfaces. Boundary-Layer Meteorol 18:373–397

Rotach MW (1993) Turbulence close to a rough urban surface. Part I: Reynolds stress. Boundary-Layer Meteorol 65:1–28

Rotach MW (1995) Profiles of turbulence statistics in and above an urban street canyon. Atmos Environ 29(13):1473–1486

Salizzoni P (2006) Mass and momentum transfer in the urban boundary layer. PhD thesis, Politecnico di Torino – Ecole Centrale de Lyon, 186 pp

Soulhac L (2000) Modélisation de la dispersion atmosphérique à l'intérieur de la canopée urbaine. PhD thesis, École Centrale de Lyon, 345 pp

Soulhac L, Puel C, Duclaux O, Perkins RJ (2003) Simulation of atmospheric dispersion in Grater Lyon: an example of the use of nested models. Atmos Environ 37:5147–5156

Takahashi H, Tejima M, Nakazato M, Fukoka Y (1996) Measurement of air circulation in an urban canyon by means of interval shooting of tracer balloons. Jpn Progress Climatol 70:129–134

Walton A, Cheng AYS, Yeung WC (2002) Large-eddy simulation of pollution dispersion in an urban street canyon – Part I: comparison with field data. Atmos Environ 36:3601–3613

Yamartino RJ, Wiegand G (1986) Development and evaluation of simple models for the flow, turbulence and pollutant concentration fields within an urban street canyon. Atmos Environ 20(11):2137–2156